Technical Notes

TECHNICAL NOTES are short manuscripts describing new developments or important results of a preliminary nature. These Notes cannot exceed 6 manuscript pages and 3 figures; a page of text may be substituted for a figure and vice versa. After informal review by the editors, they may be published within a few months of the date of receipt. Style requirements are the same as for regular contributions (see inside back cover).

Surface Curvature Effect on the Calculation of Separation Bubble

D. H. Choi* and D. J. Kang†
Korea Advanced Institute of Science and Technology, Seoul, South Korea

Introduction

THE separation bubble developed on an airfoil surface has been studied by many investigators. The computational aspect of this problem also has received considerable attention in recent years.[1-4] Most of this earlier research was pursued within the framework of the thin boundary-layer theory: the bubble region was calculated by the interactive boundary-layer technique in which the small variation in the external velocity due to the bubble was accounted for through the equivalent source distribution over the surface. This procedure has been very successful in predicting the separation bubble. The underlying approximations, however, lose their validity when the surface curvature is large, since the bubble can no longer be considered small and the Hilbert integral[2] does not adequately simulate the displacement effect.

The purpose of this Note is to present a more accurate calculation procedure that uses partially parabolized Navier-Stokes (PPNS) equations and to assess the significance of the higher-order terms in the equations. A PPNS approach is well suited to this problem since it is capable of computing the elliptic effects due to the pressure field. Also, the flow sufficiently becomes parabolic far upstream and downstream of the bubble. Therefore, the boundary conditions can be easily specified.

Solution Procedure

In a body-fitted orthogonal coordinate system, with ξ being parallel to the surface and η normal to it, the continuity and the PPNS equations are given in the following dimensionless form:

$$\frac{1}{h_1}\frac{\partial U}{\partial \xi}+\frac{1}{h_2}\frac{\partial V}{\partial \eta}+K_{21}U+K_{12}V=0 \tag{1}$$

$$\frac{U}{h_1}\frac{\partial U}{\partial \xi}+\frac{V}{h_2}\frac{\partial V}{\partial \eta}+(K_{12}U-K_{21}V)V=-\frac{1}{h_1}\frac{\partial p}{\partial \xi}-\frac{1}{h_2}\frac{\partial}{\partial \eta}(\overline{uv})$$
$$-2K_{12}\overline{uv}+\frac{1}{Re}[L_1(U)+L_2(V)] \tag{2}$$

$$\frac{U}{h_1}\frac{\partial V}{\partial \xi}+\frac{V}{h_2}\frac{\partial V}{\partial \eta}(K_{21}V-K_{12}U)U=-\frac{1}{h_2}\frac{\partial p}{\partial \eta}-\frac{1}{h_1}\frac{\partial}{\partial \xi}(\overline{uv})$$
$$-2K_{21}\overline{uv}+\frac{1}{Re}[L_1(V)-L_2(U)] \tag{3}$$

where

$$L_1=\frac{1}{h_2^2}\frac{\partial^2}{\partial \eta^2}+(K_{21}-K_{11})\frac{\partial}{h_1\partial \xi}+(K_{12}-K_{22})\frac{\partial}{h_2\partial \eta}-K_{21}^2-K_{12}^2$$

$$L_2=2\left(K_{12}\frac{\partial}{h_1\partial \xi}-K_{21}\frac{\partial}{h_2\partial \eta}\right)+\frac{1}{h_1}\frac{\partial K_{12}}{\partial \xi}-\frac{1}{h_2}\frac{\partial K_{21}}{\partial \eta}$$

$$K_{12}=\frac{1}{h_1h_2}\frac{\partial h_1}{\partial \eta},\ \text{etc.} \tag{4}$$

and where (U,V) and (u,v) are, respectively, the mean and fluctuating velocity components in the (ξ,η) directions, p the pressure, Re the Reynolds number, and h and K the metric coefficients and curvature parameters. Note that the equations retain all the higher-order curvature terms that have been neglected in other similar calculations. Although the normal Reynolds-stress terms can be retained without any difficulty, the calculations using the present turbulence model show that their contribution to the solution is insignificant, and therefore these terms are dropped from the equations.

The algebraic eddy-viscosity model of Baldwin and Lomax[5] is adopted as a closure relationship. This model uses the distribution of vorticity to determine the length scale, and therefore the location of the outer edge of a thin shear layer is not required. The simple zero-equation model is convenient, since the entire flow domain, where both laminar and turbulent regions are present, can be handled with a single set of equations.

The calculation domain is of particular importance in this analysis. It needs to be small to reduce the computation time and, yet, should be large enough so that the conditions at the boundary are not affected by the presence of the bubble. In the present analysis, the calculation starts from sufficiently far upstream of the bubble to well downstream of it where the parabolic condition has been recovered, while the outer boundary is placed far enough outside the boundary layer. The following boundary conditions are prescribed along each of these boundaries:

Upstream, $\xi=\xi_u$	U specified, $\dfrac{\partial V}{h_1\partial \xi}=0$
Downstream, $\xi=\xi_d$	$\dfrac{\partial p}{h_1\partial \xi}$ specified
Outer, $\eta=\eta_0$	U, p specified
Wall, $\eta=0$	$U=V=0$

(5)

The values of V along the outer boundary and p along the wall are determined implicitly by the governing equations. The upstream velocity profile is provided by a separate boundary-layer calculation, and the other boundary conditions are obtained from the potential flow solution.

The finite-difference scheme employed for this calculation is a simplified version of an algorithm proposed by Galpin et al.[6] The procedure is briefly outlined here. From the discretized continuity and ξ momentum equations, expressions for $U_{i,j}$ and $p_{i,j}$ are obtained in terms of the values at other grid points and the values of previous iteration step. Here, the central differencing is used except for the streamwise convective derivatives, which are discretized by upwind differencing.

Received June 7, 1988; revision received Dec. 11, 1988.

*Associate Professor, Department of Mechanical Engineering. Member AIAA.
†Graduate Student, Department of Mechanical Engineering.

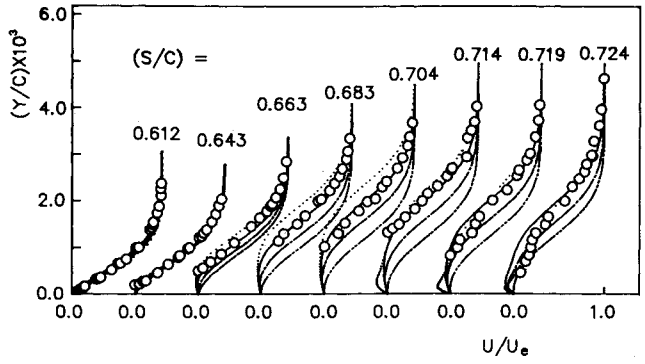

Fig. 1 Comparison of velocity profiles on the airfoil section, NACA 66_3-018, for $\alpha = 0$ deg, $Re = 2 \times 10^6$ (o data of Gault,[7] —— case 1a, · · · · · case 1b, — · · — case 2a, — · — case 2b).

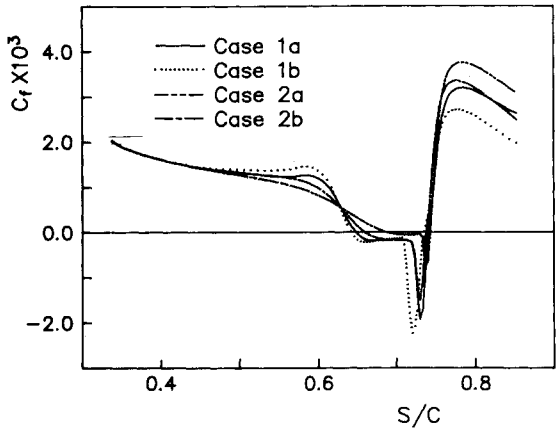

Fig. 2 Wall-shear-stress distributions for various calculations.

These expressions then are substituted for $U_{i,j}$ and $p_{i,j}$ in the η-momentum equation and a pentadiagonal system of equations for V results. These equations for V are solved simultaneously at each ξ station. Once V is obtained, U and p are readily determined from the continuity and ξ-momentum equations, respectively. After each complete sweep, the pressure field is corrected to expedite the convergence (see Ref. 6 for details). The procedure is repeated until the solution converges. Initially, the transition is triggered immediately after the separation and is gradually moved downstream as iteration progresses until the prescribed location is reached. This procedure is found to be helpful in obtaining stable convergence behavior.

Results and Discussion

The procedure described above has been used to perform calculations for the airfoil section, NACA 66_3-018, at zero incidence and Reynolds number of 2×10^6. The calculations are carried out in the domain $0.33 < s/c < 0.85$ and $n/c < 0.04$. Here, s and n denote the physical distances along and normal to the surface. This outer boundary represents about 8-10 times the maximum boundary-layer thickness in the region, and a further reduction of the domain was found to affect the solution. A 100×80 nonuniform grid is employed with the nodes concentrated close to the wall and inside the bubble.

Calculations are made first for two different boundary conditions along the outer boundary, $\eta = \eta_0$. The conditions, which are enforced as explained in Eq. (5), are the *potential flow* pressure and velocity distributions computed for case 1a along the out boundary and for case 1b along the surface. Similar calculations then are repeated with no curvature terms, which we shall denote case 2a or 2b according to the boundary conditions applied. The transition is prescribed for all four cases; the locations are $s/c = 0.721$ for both cases 1a and 2b, 0.709 for case 1b, and 0.730 for case 2a. The latter two locations are chosen to keep the bubble size comparable.

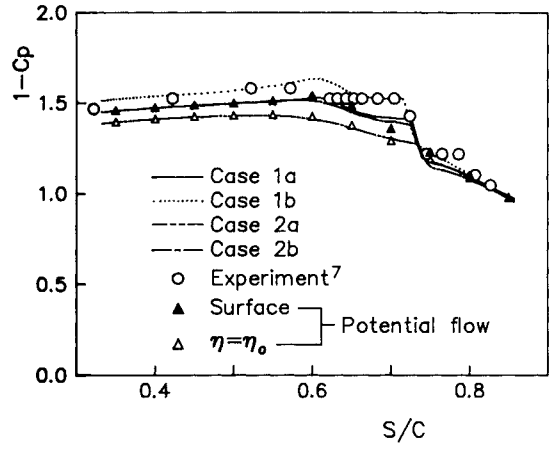

Fig. 3 Pressure distributions in the vicinity of the bubble (triangles ▲ and △ represent the potential flow pressure distributions that are used as boundary conditions).

The results are compared in Figs. 1-3. For case 1a, the velocity profiles (Fig. 1) are in very good agreement with the experimental data.[7] The boundary layer separates and reattaches at $s/c = 0.648$ and 0.741, respectively, as seen from the shear-stress distribution in Fig. 2. The surface pressure distribution (Fig. 3) follows the measured data very closely, apart from the fact that the level is slightly lower. The discrepancy noted is attributed to the use of the potential-flow condition along the outer boundary Δ. Since the general pressure level of the potential flow differs from that of the experiment, as can be seen from the figure as pointed out by Cebeci and Schimke,[2] the calculated pressure distribution is not expected to be the same as the measured one. It is also seen from Fig. 3 that the calculation identically reproduces the surface pressure of the potential flow away from the bubble. This signifies that the pressure variation across the layer is well captured in the calculation.

The use of the surface pressure and velocity distributions (case 1b) predicts an earlier separation ($s/c = 0.642$, Fig. 2) and more rapid growth of the bubble that, in turn, triggers an earlier transition. The result is quite different from that of case 1a: a relatively thicker bubble. On the other hand, the calculations without the curvature terms in both cases 2a and 2b give a later separation. The bubbles are thinner and shorter. Of the two, the result of case 2b is closer to the experiment than the other: the pressure distribution is nearly identical with that of case 1a.

From these calculations, one can make following observations. The difference between the results of cases 1a and 2a suggests that the curvature terms play an important role. It is evident that these terms should not be neglected in order to capture the pressure variation across the domain. On the other hand, the difference in cases 1a and 1b implies that the surface condition is not a proper boundary condition unless the domain is sufficiently thin. It is interesting to see that case 2b gives a better result than case 2a. This seems to indicate that imposing the surface pressure along the outer boundary tends to compensate for the missing curvature effect to some extent. Judging from the above observations together with the fact that the present calculation domain is near midchord, where the curvature is of relatively small magnitude, the curvature effect, in general, is not negligibly small for calculation of the separation bubble. The Hilbert integral type of pressure correction used in the interactive boundary-layer calculation will also become less accurate as the bubble and the curvature become larger. It is, therefore, necessary to use the PPNS equations with the higher-order terms, especially near the leading edge.

Conclusions

The separation bubble developed on an airfoil surface is successfully calculated using a PPNS procedure with the boundary condition that is free of bubble influences. Inclusion of the higher-order curvature terms in the equations, in combination with the proper outer boundary condition, is found necessary to get the desired results.

Acknowledgments

This work was supported by the Korea Science and Engineering Foundation. The authors are grateful to the reviewers for their valuable comments.

References

[1]Briley, W. R. and McDonald, H., "Numerical Prediction of Incompressible Separation Bubbles," *Journal of Fluid Mechanics,* Vol. 69, Pt. 4, June 1975, pp. 631-656.

[2]Cebeci, T. and Schimke, S. M., "The Calculation of Separation Bubbles in Interactive Tubulent Boundary Layers," *Journal of Fluid Mechanics,* Vol. 131, June 1983, pp. 305-317.

[3]Vatsa. V. N. and Carter, J. E., "Analysis of Airfoil Leading Edge Separation Bubbles," *AIAA Journal,* Vol. 22, Dec. 1984, pp. 1697-1704.

[4]Kwon, O. K. and Pletcher, R. H., "Prediction of Subsonic Separation Bubble on Airfoils by Viscous-Inviscid Interaction," *Proceedings of a Symposium on Numerical and Physical Aspects of Aerodynamic Flows III,* edited by T. Cebeci, Springer-Verlag, New York, 1984, pp. 163-171.

[5]York, B. and Knight, D., "Calculation of Two-Dimensional Turbulent Boundary Layers Using the Baldwin-Lomax Model," *AIAA Journal,* Vol. 23, Dec. 1985, pp. 1849-1850.

[6]Galpin, P. F., Van Doormaal, J. P., and Raithby, G. D., "Solution of the Incompressible Mass and Momentum Equations by Application of a Coupled Equation Line Solver," *International Journal of Numerical Methods in Fluids,* Vol. 5, July 1985, pp. 615-625.

[7]Gault, D. E., "An Experimental Investigation of Regions of Separated Laminar Flow," NACA TN 3505, Sept. 1955.

Evaluation of the Gradient Model of Turbulent Transport Through Direct Lagrangian Simulation

Peter S. Bernard* and Mohamed F. Ashmawey†
University of Maryland, College Park, Maryland
and
Robert A. Handler‡
Naval Research Laboratory, Washington, D.C.

Introduction

THE mean gradient, or eddy viscosity, model of momentum transport has been an essential component of a wide range of closure schemes.[1] Many of these have achieved some significant successes, particularly in the prediction of relatively simple shear flows such as those in channels, pipes, or nonseparating boundary layers. In spite of these accomplishments, substantial questions remain concerning the fundamental validity of the approach. Criticisms of the gradient law extend back at least to Taylor,[2,3] who thought that its basic premise, that momentum would be conserved on particle paths over a mixing length, failed to account realistically for the likely effect that pressure forces would have on the motion of fluid particles. Later Corrsin[4] showed that the circumstances under which gradient transport could be trusted are more restrictive than the conditions usually found in practice. In particular, the length scale of turbulent mixing is often comparable to that over which the gradient field varies. A detailed analysis of gradient transport also has been provided by Tennekes and Lumley,[5] who have pointed out its incompatibility with the accepted belief that Reynolds stress is produced mostly in coherent events involving vortical structures.

The limitations of the eddy viscosity model appear to surface more clearly in the case of complex flows,[6] where the level of performance of many closure schemes depending on it has been less than satisfactory. Presumably, in this instance essential nongradient processes in the physics of turbulent transport cannot be neglected. A well-known example of this is the wall jet flow,[7] where the gradient model is fundamentally at odds with the observed mean velocity and Reynolds shear stress fields.

To date, previous analyses of turbulent momentum transport have had to rely, in varying degrees, on heuristic arguments, since the Reynolds stress does not lend itself readily to formal treatment by the usual statistical techniques. It is of some interest, therefore, to develop a method of testing the gradient transport hypothesis that is purely formal, i.e., involving no assumptions.

In this Note, a Lagrangian expansion of the Reynolds shear stress is introduced that, in principle, allows for a precise test of the gradient transport model. An analogous construction for the case of vorticity transport has been used previously in developing closure schemes.[8-10] The implementation of this analysis requires evaluation of the terms in the expansion by ensemble averaging over a data file of Lagrangian particle paths. For the present study the necessary paths were obtained at two locations near the boundary from a direct numerical simulation of turbulent channel flow.[11] The results confirm that the most significant source of nongradient transport arises from the influence of the pressure field. Of somewhat less importance, but significant nonetheless, are higher-order effects originating from transport on a scale greater than that of linear variation in mean velocity.

Analysis of Gradient Transport

It is desirable to explain the source of correlation in $\overline{uv}$ at a particular point $\boldsymbol{a}$ at time t_0. Here and henceforth, u, v, and w represent the streamwise, wall-normal, and spanwise velocity fluctuations, respectively, in a channel flow; $\overline{U}$ is the mean streamwise velocity, $U = \overline{U} + u$, and the overbar denotes an ensemble average. Consider a fluid particle with trajectory $\boldsymbol{x}(\boldsymbol{a},t)$ that is known to be at point $\boldsymbol{a}$ at time t_0, i.e., $\boldsymbol{x}(\boldsymbol{a},t_0) = \boldsymbol{a}$. Henceforth, the given point $(\boldsymbol{a},t_0)$ will be denoted as point $\boldsymbol{a}$ while the position occuring earlier in time along the path, at $t = t_0 - \tau, \tau > 0$, is denoted as point b. In contrast to point $\boldsymbol{a}$, point b varies randomly from realization to realization of the turbulent field.

Integration of the U component of the Navier-Stokes equation along $\boldsymbol{x}(\boldsymbol{a},t)$ from b to $\boldsymbol{a}$ yields

$$U_a - U_b = -\int_{t_0-\tau}^{t_0} \nabla p \, ds + \int_{t_0-\tau}^{t_0} \frac{1}{R} \nabla^2 U \, ds \qquad (1)$$

which indicates that the momentum of the fluid particle changes along the path due to the accumulated action of the pressure and viscous forces. Here R is an appropriate Reynolds number, p is the nondimensional pressure field, and subscripts $\boldsymbol{a}$ and b denote quantities evaluated at points $\boldsymbol{a}$ and b, respectively.

Expressions U_a and U_b in Eq. (1) may be decomposed into $U_a = \overline{U}_a + u_a$ and $U_b = \overline{U}_b + u_b$, where it should be noted

Received June 22, 1988; revision received Dec. 20, 1988.

*Associate Professor, Department of Mechanical Engineering.

†Graduate Research Assistant, Department of Mechanical Engineering.

‡Research Engineer, Laboratory for Computational Physics and Fluid Dynamics.